Design of a distributed optical fiber sensor system for measuring immersed tunnel joint deformations

Zhang, Xuehui; Broere, Wout

DOI
10.1016/j.tust.2022.104770

Publication date
2023

Document Version
Final published version

Published in
Tunnelling and Underground Space Technology

Tunnelling and Underground Space Technology 131 (2023) 104770

Contents lists available at ScienceDirect

Tunnelling and Underground Space Technology incorporating Trenchless Technology Research

journal homepage: www.elsevier.com/locate/tust

Design of a distributed optical fiber sensor system for measuring immersed tunnel joint deformations

Xuehui Zhang , Wout Broere *

Geo-Engineering Section, Department of Geoscience and Engineering, Delft University of Technology, Delft, the Netherlands

ARTICLE INFO

Keywords:
Immersed tunnel
Joint deformation
Distributed optical fiber sensor

ABSTRACT

Monitoring the deformations of immersed tunnels is important during the entire tunnel service life to assess the structural integrity of the tunnel. Conventional joint deformation monitoring is based on manual levelling measurements and normally occurs only at multi-year intervals, which does not allow to capture short term deformation behavior. In this study a new joint monitoring system using distributed optical fiber sensors (DOFS) is developed. A special sensor layout is designed that allows simultaneous measurements of both horizontal joint opening and vertical uneven settlement of the immersion and dilation joints. For this sensor scheme the transfer relation from fiber strain to joint deformation is derived and verified by in-lab experiments. The sensor system proves to be able to detect sub-millimeter joint deformations, indicating a more than sufficient accuracy for structural monitoring of immersed tunnel joints. Subsequently, the First Heinenoordtunnel in the Netherlands is instrumented using this distributed optical fiber sensing system, in order to obtain additional data for both long-term and short-term assessment of its structural condition.

1. Introduction

Immersed tunnels have been used in many places worldwide to cross waterways, and can be quite favorable when compared with a bridge or bored tunnel . Since the first immersed tunnel constructed in 1910s, there are now over 150 immersed tunnels in use worldwide (Lunniss and Baber, 2013). In the Netherlands alone, there are over 25 immersed road and rail tunnels in service, with the oldest the Maastunnel in Rotterdam, which was opened in 1942.

Longitudinally, immersed tunnels feature a chain of jointed segments underwater. The construction process of immersed tunnels follows a general “trenching - segment prefabrication - element transport - immersion” procedure (Saveur and Grantz, 1997). A typical segmented immersed tunnel generally has two types of joints - immersion joints (or element joints) and dilation joints (or segment joints) (Lunniss and Baber, 2013). The structural segmentation makes immersed tunnels more adaptable to effects of longitudinal uneven settlements, as compared to a continuous non-jointed structure. Because individual segments have a high degree of independence in following deformations, relative deformation is more likely to occur at the joints. In general, this reduces the stress development due to uneven settlement in the segment body, at the expense of localizing these deformations in the joints.

The deformation occurring at the joint, if it remains limited, should not deteriorate the structural safety and hence be acceptable, but unfortunately the design assumptions for many immersed tunnels started from rather limited allowed lifespan settlements. Long-term settlements observed for several immersed tunnels exceed these design limitations, which may signal unfavorable structural load conditions and an increased risk of structural safety issues. Independent movement of adjoining segments generally causes joint openings, uneven settlements and lateral drift, which are all closely related to both structural safety and watertightness. For example, the Shanghai outer-ring expressway tunnel in China, an immersed tunnel on soft ground, was observed to have an unexpectedly large joint closure which caused excess compression and damage of the GINA gasket (Bai and Lu, 2016). The Kiltunnel in the Netherlands also shows a significant uneven settlement (as high as 70 mm, approximately 10 times the maximum design assumption) longitudinally, and at one dilation joint concrete cracking and significant joint leakage were observed (Gavin et al, 2019). More settlement data for some early immersed tunnels worldwide can be found in Grantz (2001) and Wang et al. (2020), and it should be noted that structural safety issues, like local concrete cracking, damage of rubber waterproof gaskets and joint leakages due to excessive joint

* Corresponding author at: Geo-Engineering Section, Delft University of Technology, Stevinweg 1, 2600 GA Delft, The Netherlands.
E-mail address: W.Broere@tudelft.nl (W. Broere).

https://doi.org/10.1016/j.tust.2022.104770
Received 11 August 2021; Received in revised form 27 May 2022; Accepted 21 September 2022
Available online 10 October 2022

deformation occur more frequently than desired and should gain more attention during tunnel design and service life.

Despite this high necessity to monitor joint deformations, conventional monitoring practice is behind both in terms of measuring accuracy and frequency. Deformation monitoring of immersed tunnels is in most cases still limited to vertical settlement monitoring by manual levelling, measured at yearly or multi-year intervals. Longitudinal and lateral segment movement are rarely investigated due to difficulties in obtaining reliable measurement as well as a lack of suitable and unobtrusive measuring techniques. The limitations of conventional monitoring practices have been shown in several tunnel projects (Berkhout et al., 2014; van Montfort, 2018; Bai and Lu, 2016), and this further highlights the need for a monitoring system that is capable of providing information for structural safety evaluations.

Distributed optical fiber sensor (DOFS) is a relatively new type of sensing technique which has been used more and more in structural monitoring. By attaching a continuous optical fiber to the target structure, the strain or temperature along the fiber axis can be obtained with a signal interrogator. Also, the sensing part of the optical fiber can be attached to the target structure while the fiber is extended to a remote-control data-taking system some distance away from the observed structure itself, which is especially useful for cases where the monitoring location is mostly inaccessible. In geotechnical engineering, DOFS has been used to monitor, for example, pile strain and tunnel lining deformation. Gue et al. (2015) used DOFS to monitor the behavior of an existing cast iron segmented tunnel, where the fiber was glued continuously along the section circumference and point-fixed at circumferential joints. Similar studies can be found in Mohanad et al. (2010); Acikgoz et al. (2017) and Wang et al. (2018). Such studies have shown the advantages of DOFS over localized point sensors (like strain gauges), as well as their high potential in structural health monitoring.

This study aims to design a DOFS system for immersed tunnel joint monitoring and assess the sensing system performance experimentally. For the first time, DOFS is used in a joint deformation monitoring system which fulfills high-frequency and remote-control data-taking requirements. This paper will first discuss the deformation mode of immersed tunnel joints and provide a brief introduction of the DOFS adopted, followed by the description of a sensor layout design that allows for joint deformation monitoring along multiple axes of displacement, as well as the joint displacement-fiber strain transform relations. Subsequently this sensor layout is verified with in-lab experiments and the accuracy and reliability of the method are determined. Finally, the validity of the method in field conditions is shown in a field installation case study in the First Heinenoordtunnel.

2. Deformation patterns of immersed tunnel joints

2.1. Dilation joints

Dilation joints (or segment joints) are located between adjoining segments within an immersed tunnel element. A typical immersion element is over 100 m long and is manufactured in segments of 20 to 25 m each in the dry-dock for ease of concreting and to limit shrinkage cracks due to thermal expansion directly after casting. For watertightness, a special steel-rubber gasket water-stop is embedded in the segment body during casting and crosses the dilation joint gap, see Fig. 1 (a). The individual segments that form an immersion element are temporarily pretensioned with longitudinal tension bars, and transported to the site for subsequent immersion. The concrete collar at segment ends provides interlocking and allows for shear force transfer between adjoining segments, see Fig. 1(a).

Cyclic opening and closure of the dilation joints may deteriorate the integrity of the rubber gasket and induce leakages in the tunnel, while uneven settlements between segments may trigger a significant shear force in the collar which may damage the gasket and the concrete body directly, see Fig. 1(b). Commonly observed problems at dilation joints are leakages and local concrete cracking due to high stress concentrations. For example, a serious water inflow was found at dilations joint of the Kiltunnel and the First Coentunnel in the Netherlands, and concrete cracking has also been observed in the Kiltunnel related to the excessive vertical relative deformation (Van Montfort, 2018; Gavin et al, 2019). The lateral drift at dilation joints is rarely monitored and hence it remains unclear if this contributes significantly to collar damage. For the purpose of monitoring structural safety of these joints, the joint opening and uneven vertical settlements should form the minimum aspects to be measured during the service life of the tunnel.

2.2. Immersion joint

Immersion joints (or element joints) are the joints formed when two elements are connected during immersion. A typical immersion joint has a different profile than a segment joint, with an outside flange on which a GINA profile is attached prior to immersion. On the inside of the element a larger gap (compared to the dilation joint) is provided that allows for the installation of a water-stop gasket (OMEGA profile), horizontal and vertical shear keys and external cover boards, see Fig. 2 (a).

During the immersion process, the GINA gasket is compressed to isolate the inside of the tunnel from the surrounding water and works as a temporary water-stop. Later on the OMEGA profile is installed internally as the primary water barrier. As these rubber gaskets have a lower axial and shear stiffness than the concrete body of the tunnel, they do not provide significant shear resistance at the immersion joints. Special shear keys are installed in the joint gap which provide shear resistance in case of uneven settlements after immersion. Usually a small gap at the interface of the shear key with the concrete body allows for small relative displacements both vertically and transversely before the shear key is activated.

Immersion joints will compress and relax somewhat during normal operation, as the tunnel elements extend and shrink with changes in temperature, and the resulting deformation normally is compensated at the immersion joints (Rahadian et al., 2018). A limited joint opening or compression at which the GINA profile remains pre-stressed is acceptable, but over-compression of the GINA profile beyond limit values may

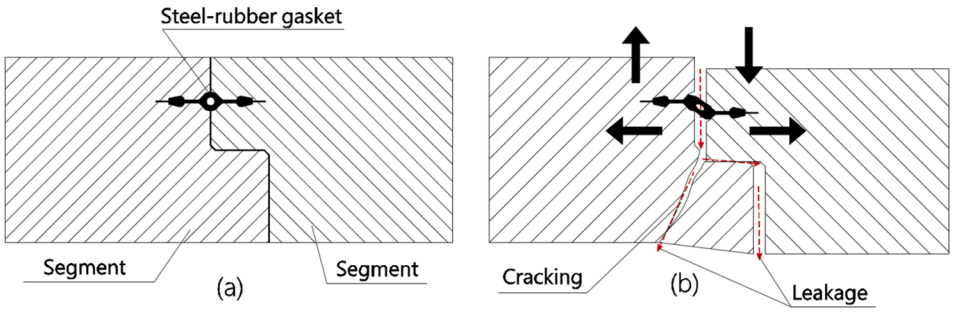

Fig. 1. Dilation joint deformation at tunnel roof: (a) schematic of a typical dilation joint and (b) deformed joint.

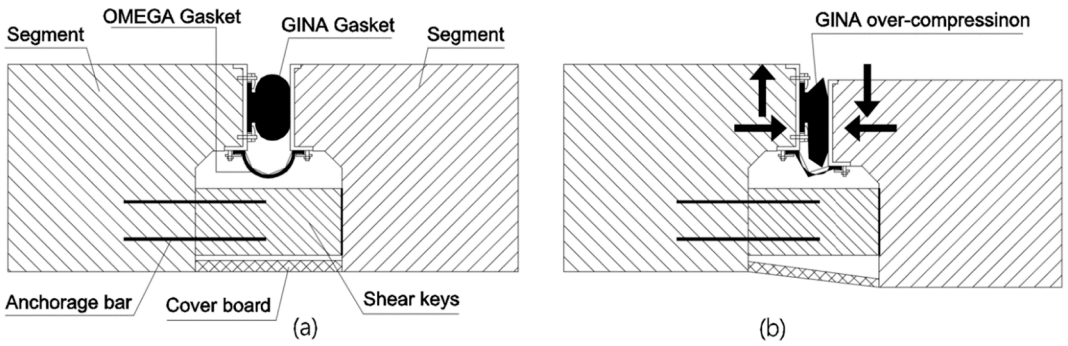

Fig. 2. Immersion joint deformation at tunnel roof: (a) Schematic of a typical immersion joint and (b) deformed joint.

cause gasket damage (Bai and Lu, 2016), and at extreme joint opening the lack of prestressing at the contact between the element and the GINA may lead to leakages, see Fig. 2(b). In addition, significant uneven settlement may occur if the vertical shear keys don't function properly. For an immersed tunnel on soft ground, unexpected joint gap offsets were found on the sidewalls at the upstream and downstream sides (Li et al, 2011), which potentially indicates segment transverse drift is also possible, see Fig. 3. However, it should be noted this segment body drift is not caused by a concentrated transverse shear displacement at the joint, but by a rotation or tilt along the foundation plane which causes uneven joint opening and closure.

In summary, available monitoring has shown at least a 2-directional deformation mode can occur at the immersion joints, consisting of vertical uneven settlement of two sides of the joint and a horizontal joint opening or closure, see Fig. 2(b). A competent joint monitoring system should be able to detect both these deformation modes.

3. Design of a distributed optical fiber sensor system for measuring joint deformations

3.1. Introduction of distributed optical fiber sensors

The Brillouin frequency shift Δf (BFS) of the backscattered light within an optical fiber, is linearly dependent on the fiber strain (ε) and temperature change (ΔT) (Ohno et al., 2001; López-Higuera et al., 2011; Motil et al., 2016), as shown in Eq. (1):

$$\Delta f = C_\varepsilon \varepsilon + C_t \Delta T \tag{1}$$

where $C_\varepsilon \wedge C_t$ are strain and temperature sensitivity coefficients, which are constant properties of the optical fiber. By decoupling the temperature component $C_t \Delta T$, the strain distribution along a fiber cable can be obtained.

A DOFS system that uses this principle consists of a continuous optical fiber (as a sensing fiber) plus a signal interrogator, see Fig. 4. The optical fiber is attached to the monitored structure, acting as both a sensor and a signal transmission medium, while the fiber end (one end or both ends) is plugged into the interrogator. According to different signal-processing principles, commercially available (Brillouin scattering) interrogators for structural monitoring can be classified as: Brillouin Optical Time Domain Reflectometry/Analyzer (BOTDR/A); Brillouin Optical Frequency Domain Reflectometry/ Analyzer (BOFDR/A), and others, see López-Higuera et al., (2011) and Motil et al., (2016) for more details.

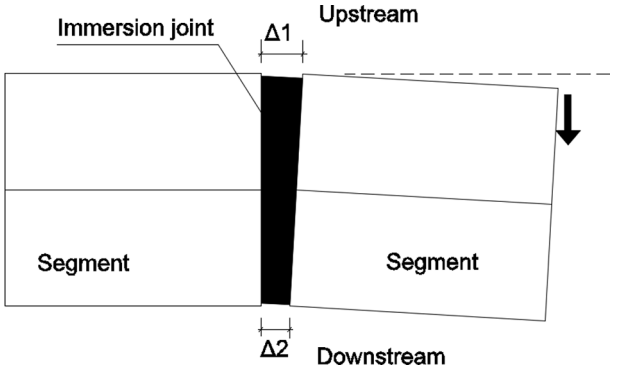

Fig. 3. Transverse drift of segment body (top view).

3.2. Optical fiber sensor layout

In DOFS monitoring, a continuous sensing optical fiber is attached to the structure or area of interest, and (one or both) fiber ends extend to the interrogator. It should be noted that DOFS only obtains the axial strain (after decoupling the temperature effect) in the direction of the fiber. For some monitoring tasks, this distributed axial strain is the desired observable, for instance when the sensing fiber is embedded into the structure or continuously bonded on structure surface. For example, optical fibers can be embedded into concrete piles or secant walls for vertical strain measuring (Pelecanos et al, 2018; Schwamb et al, 2014), or bonded continuously on structure surfaces for strain monitoring (Gue et al. 2015).

However, for immersed tunnel monitoring the interest lies more in the localized displacements and deformations at specific locations along the tunnel and less in the strain along the segment bodies. Therefore, the sensing fiber needs to be installed in a special layout so as to effectively detect the anticipated displacements. In this case, the observable displacement is indirectly derived from the local fiber strain, and an effective sensing layout design should take into account: the potential displacement range, a distinct and unique fiber strain to displacement transfer relation, and ease of sensor installation. A simple sensing layout for displacement measurements can consist of a short length (gauge length) of fiber cable fixed at two points, and the relative displacement between these points can thus be monitored and calculated. For example, Wang et al. (2018) and Zhu et al. (2022) utilized an optical fiber sensor (a single gauge length) to measure bored tunnel joint openings, by point-fixing the sensing fiber (with 1.2 m gauge length) at two sides of the joint. Mohanad et al. (2010) used optical fibers to detect potential global deformation patterns of an old masonry tunnel during close-proximity construction activities, where the continuous fiber was fixed at several discrete points of a tunnel cross-section.

In order to detect the two-directional joint displacement (both joint opening and vertical uneven settlement), more gauge lengths are needed and aligned in a way which can transfer displacement to fiber strain effectively. Also, in order to detect both extension and contraction, pre-tensioning of the fiber is usually needed during optical fiber installation. As an additional requirement, the sensing fiber layout should be designed in such a way as to reduce the field installation difficulty as much as possible, which means a uniform layout for all monitored joints is preferred. These requirements have resulted in a sensor layout design

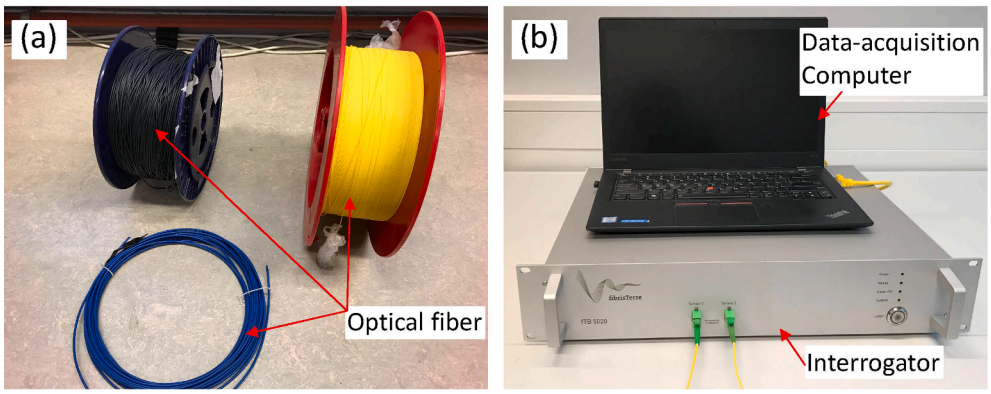

Fig. 4. Components of the DOFS system:(a) optical fiber (b) interrogator(BOFDA) with data-acquisition computer.

as shown in Fig. 5, and the transfer relation between fiber strain and joint displacement for this layout is derived below.

At each joint, two short sections of the optical fiber lines (FLs) are fixed at 3 points, see fixation points FP1 to FP3 in Fig. 5. The two sensing fiber lines (FL1 and FL2) plus 3 fixation points form a sensor triangle (or sensor block) which detects two-directional joint displacements (joint opening along Y-axis and vertical uneven settlement along Z-axis). During installation, FL1 is oriented horizontally and FP1 and FP3 are aligned on a vertical line (along the Z-axis in Fig. 5).

The deformation of the horizontal fiber line FL1 can be described using Eq. (2) to (4) below, assuming that FL1 only detects horizontal deformations, which simplification is valid as the impact of any vertical deformations on the strain in FL1 is negligible.

$$\varepsilon_{1.0} = \frac{\Delta f_{1.0}}{c_\varepsilon} \tag{2}$$

$$l_{1.0} = l_1(1+\varepsilon_{1.0}) \tag{3}$$

$$\Delta y_0 = l_1 \varepsilon_{1.0} \tag{4}$$

For the inclined fiber line FL2, the following geometrical relation is found:

$$\varepsilon_{2.0} = \frac{\Delta f_{2.0}}{c_\varepsilon} \tag{5}$$

$$l_{2.0} = l_2(1+\varepsilon_{2.0}) \tag{6}$$

and the height difference between FP1 and FP3 is given as:

$$h_0 = \sqrt[2]{l_{2.0}^2 - l_{1.0}^2} \tag{7}$$

where l_1/l_2 are the sensor lengths of the horizontal (FL1) and inclined (FL2) fiber lines; $l_{1.0}/l_{2.0}$ are the lengths of FL1/FL2 at the time of installation; $\Delta f_{1.0}/\Delta f_{2.0}$ are the measured Brillouin frequency shifts of FL1/FL2 at the time of installation (after decoupling the temperature component); c_ε is the strain coefficient of the sensing fiber; $\varepsilon_{1.0}/\varepsilon_{2.0}$ are the initial strains of FL1/FL2 at the time of installation ; Δy_0 is the extension due to prestraining of FL1 at the time of installation; and h_0 is the height difference of FP2 and FP3 at installation.

When a certain displacement along the Y and Z axis has occurred over the joint, Eqs. (2) to (7) still hold for this working state, assuming a negligible impact of second order effects on the horizontal strain. If a measurement is made at interval i, the relation between fiber strain and deformations for FL1 can be established as:

$$\varepsilon_{1,i} = \frac{\Delta f_{1,i}}{c_\varepsilon} \tag{8}$$

$$l_{1.i} = l_1\left(1+\varepsilon_{1,i}\right) \tag{9}$$

$$\Delta y_i = l_1 \varepsilon_{1.i} \tag{10}$$

For FL2, it follows that:

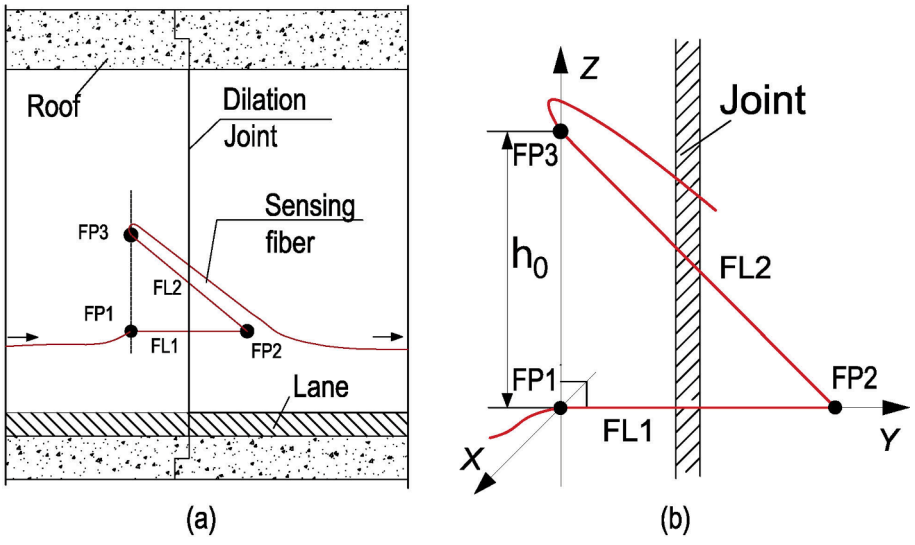

Fig. 5. Sensor layout for joint two-directional displacement measurement:(a) Field layout;(b) Installation status.

$$\varepsilon_{2,i} = \frac{\Delta f_{2,i}}{c_\varepsilon} \tag{11}$$

$$l_{2,i} = l_2(1 + \varepsilon_{2,i}) \tag{12}$$

and the height difference between FP1 and FP3 is given by:

$$h_i = \sqrt[2]{l_{2,i}^2 - l_{1,i}^2} \tag{13}$$

where $l_{1,i}/l_{2,i}$ are the lengths of FL1/FL2 at interval i; $\Delta f_{1,i}/\Delta f_{2,i}$ are the measured Brillouin frequency shifts of FL1/FL2 at interval i (decoupling temperature component); $\varepsilon_{1,i}/\varepsilon_{2,i}$ are the measured strains of FL1/FL2 at interval i; Δy_i is the extension of FL1 at interval i; and h_i is the height difference between FP1 and FP3.

If a reference measurement is obtained right after installation, the differential joint opening Δy and uneven settlement Δz at interval i, relative to the baseline status, can be calculated as:

$$\Delta y = \Delta y_i - \Delta y_0 \tag{14}$$

$$\Delta z = h_i - h_0 \tag{15}$$

It is noted that potential transverse displacements Δx also cause strains in the sensor fibers. However, as for most optical fibers the maximum allowable strain is below 1.2%, under normal working conditions, the effects of a transverse displacement Δx on the measured fiber strain only results in negligible second order effects and an ignorable error well below 0.1%. Hence the derived relation between actual displacements and measured strain is a reasonable basis to obtain joint displacements.

The analysis above shows that a sensor block, consisting of 2 fiber lines fixed at 3 discrete points at a joint, works effectively to detect two-directional joint displacements. For field applications, one potential sensor installation scheme is shown in Fig. 6, where only the sidewall of the tunnel is instrumented. Theoretically, two sensor blocks installed at both the tunnel wall and roof of the same joint could measure all 3 directions of joint displacement (Δx, Δy, Δz) simultaneously. However, sensor installation on the tunnel roof is often difficult or even impossible due to limited access and the extended traffic closures that would be required for installation, but nonetheless it is possible for instance in utility or escape ducts.

4. Verification of the sensor principle

4.1. Experiment setup description

In order to verify the reliability of the designed sensor setup, a number of in-lab experiments is performed first. These experiments aim to check whether the anticipated displacement range can be measured reliably; what the maximum allowable strain of the optical fiber is before errors become too large, and before the fiber is destroyed; and what the axial stiffness of the optical fiber is, which is especially important when pre-tensioning is required during fiber installation. A low axial stiffness usually indicates that the al fiber is fragile and tends to break easily even under normal operation conditions, whereas a high stiffness makes the sensing fiber difficult to be pre-tensioned and fixed during installation.

In the lab experiment, two types of optical fiber were selected: a polyurethane sheath fiber type NZS-DSS-C07 with a diameter of 2 mm (D-2 mm), and a tight-buffered sensing fiber type NZS-DSS-C09 with a diameter of 0.9 mm (D-0.9 mm). Both are manufactured by Nanzee Sensing Company from Suzhou, China. The strain sensitivity coefficients of the D-2 mm and D-0.9 mm fiber are tested as 48.55 MHz/0.1% and 49 MHz/0.1% respectively. A BOFDA interrogator, type fTB5020 (shown in Fig. 4(b)) and manufactured by fibrisTerre Systems GmbH, is used to measure the Brillouin frequency shift of the sensing fibers at each displacement step. This BOFDA device has a stated spatial resolution of 0.2 m (up to 2 km) and 0.5 m (up to 25 km), a spatial accuracy of 0.05 m, and fiber strain accuracy of 2 micro-strain (0.0002%), according to fibrisTerre (2021).

Fig. 7 and Fig. 8 show the joint model test setup. Important parts of the setup are:

(1) a movable platform, which consists of two wood plates, marked as bottom plate (BP) which controls the horizontal movement, and a vertical plate (VP) which allows for vertical movement. The BP and VP are assembled perpendicularly with adjustable clamps (AC), and can be fixed in place with tension screws, while they still can be moved independently by adjusting the AC.

(2) a fixed platform and fixed frame. The sensor fiber is attached to the fixed frame at two fixture points (FP1 and FP3 in Figs. 7 and 8), while fixture point 2 (FP2) is at the edge of VP. Note that the fixed platform also serves as the reference plane on which the BP slides.

(3) a sensor fiber. The selected sensor fiber is fixed at 3 points (FP1/FP2/FP3) with epoxy glue, while the fiber lines between (fiber line 1 and 2, see FL1/FL2 in Fig. 8) span the joint gap and function as deformation sensors. The two fiber lines (FL1/FL2) plus 3 fixture points (FP1/FP2/FP3) form a sensor block at the joint, and both fiber ends are extended to the BOFDA interrogator. In the lab experiment both the D-0.9 mm and D-2 mm optical fiber are attached to the fixed frame at the two sides of VP, front and back, to form two parallel sensor triangles, see Fig. 8.

(4) a number of displacement gauges. The measuring gauges include two dial gauges at the VP to measure vertical displacement ΔZ (indicated as VG1/VG2 in Fig. 8), and two dial gauges at the fixed platform (just in front of the BP) to measure horizontal displacement ΔY (indicated as HG1/HG2 in Fig. 8). All gauges have an accuracy of 0.01 mm. The use of two parallel gauges can help to reduce tilting at each displacement step in each direction.

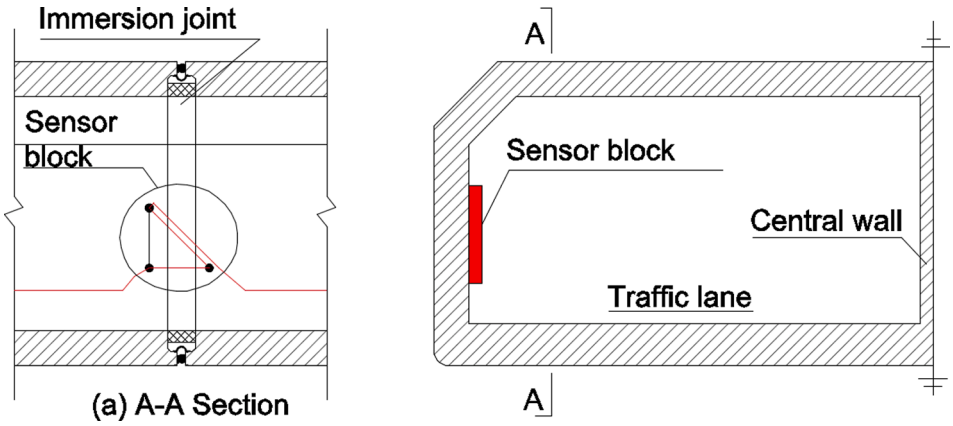

Fig. 6. Fiber layout for potential 2 directional joint deformation monitoring.

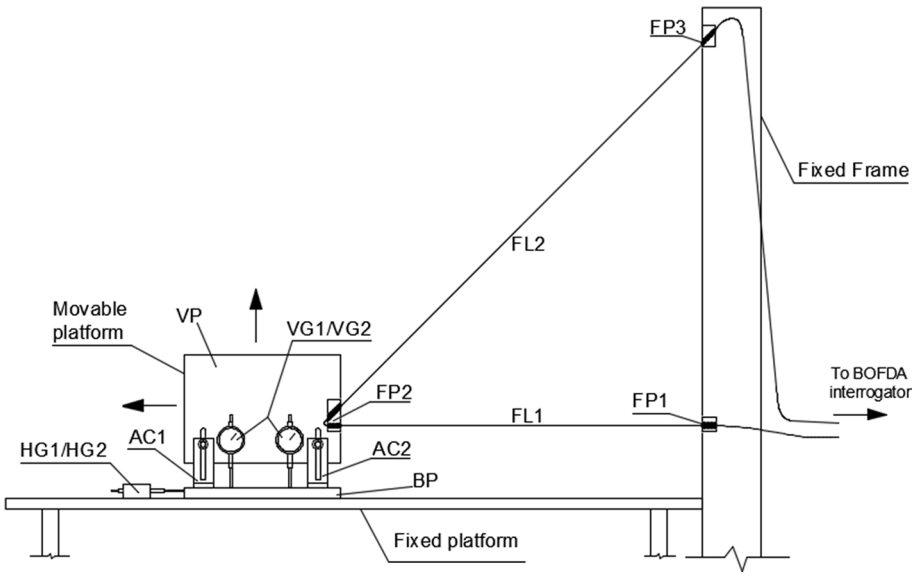

Fig. 7. Joint model displacement test set-up.

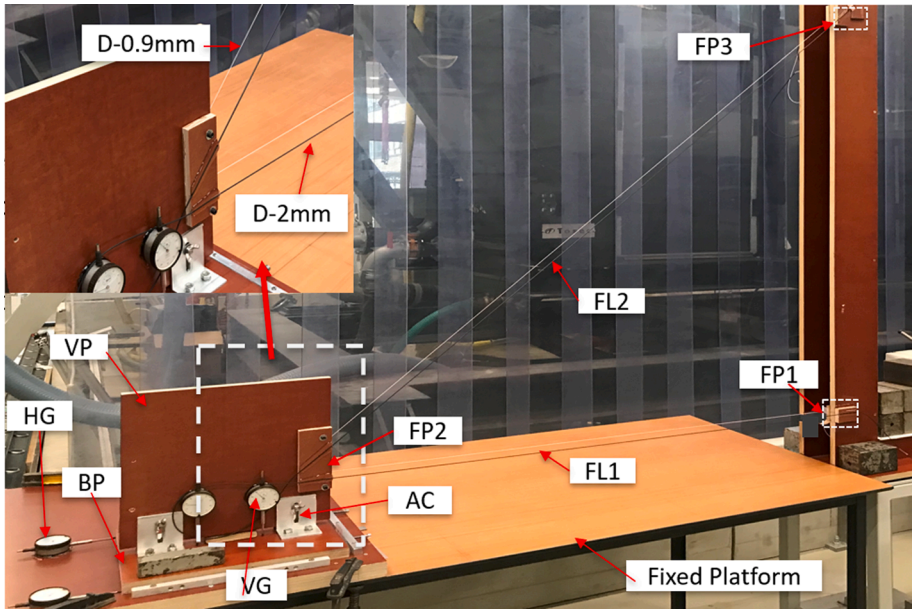

Fig. 8. Lab verification experiment set-up.

As this verification experiment is designed to verify future application of the designed sensor setup in the First Heinenoordtunnel, the parameter selection is kept consistent with the actual tunnel joint dimensions, where the immersion joint gap is between 1 m and 1.4 m wide. The parameters of the sensor block are listed in Table 1.

The movable platform is first set at a pre-strain displacement of 7 mm to provide the initial installation status, and then moved forward or backward to simulate various deformation modes. Different combinations of joint opening and closure and differential settlement can be thus modelled. The imposed ΔY can be directly read on the two HGs. The vertical plate height can be adjusted to model joint differential settlements, and at each displacement step, the vertical displacement is read directly from the two VGs. Equations (2) to (14) are used to transfer the measured Brillouin frequency shift to displacements. At each displacement step, the VP is first adjusted to impose a certain vertical displacement ($0mm, \pm 1mm, \pm 3mm, \pm 5mm$ and secondly a horizontal displacement is imposed to the BP with increments of 1 mm.

Table 1
Parameters of joint model setup.

Parameters	Value
Gauge length FL1	1200 mm
Gauge length FL2	1693 mm
Height difference at installation	1200 mm
Anticipated joint displacement range	Opening $\Delta Y(-6mm, 6mm)$
	Uneven Settlement $\Delta Z(-5mm, 5mm)$

4.2. Experimental results

The measured displacements from the optical fiber sensors are compared with the imposed displacements as obtained from the dial gauges, and potential errors are analyzed.

First the results are analyzed for strain combinations with an imposed downward vertical displacement of $\Delta Z = 0$, 1, 3 or 5 mm,

where positive vertical displacement ΔZ indicates that FP2 moves downwards. The results of each loading step are shown in Figs. 9 to 14. ΔY-Ref indicates the imposed (reference) displacement read from dial gauges, and negative ΔY values indicate a joint closure whereas positive values indicate joint opening or additional strain imposed on the fiber.

Fig. 9 shows the experimental results of the thin D-0.9 mm optical fiber when ΔZ = 5 mm, and it can be seen that the measured ΔZ is smaller than the imposed 5 mm, while the maximum gap is about 0.23 mm (when ΔZ = 4.77 mm). For the joint opening and closure, a maximum relative error of 9% is detected when ΔY = 1.09 mm (ΔY-Ref = 1 mm), and most displacement steps show a maximum relative error of below 3%, which indicates the measuring accuracy is acceptable for field monitoring. However, the D-0.9 mm fiber is found very fragile and will not be adopted in the actual field test. Therefore, only the experimental results of the D-2 mm optical fiber are further analyzed in detail here, as this type of fiber will also be used in subsequent field monitoring.

The results for the D-2 mm optical fiber are:

The reference test with ΔZ = 0 mm, where no vertical settlement is imposed, ΔY shows a maximum relative error of 4%, as shown in Fig. 10, when a measured ΔY = 1.04 mm is compared with the imposed displacement ΔY-Ref of 1 mm. This Figure also shows that when the bottom plate (BP in Fig. 8) is moved horizontally, the measured vertical settlement varies a little, which indicates that second order effects neglected in the fiber strain derivation do play a role or that limitations exist that prevent from in keeping the lab setup completely horizontally aligned. A maximum error of 0.63 mm is observed when ΔY-Ref = 6 mm. However, it should be noted that, as this is the baseline, uneven settlement relative to this baseline measured in subsequent displacement tests is a more important indication of accuracy.

For ΔZ = 1 mm, as shown in Fig. 11, a maximum relative error of 2.5% occurs, where an imposed displacement of 6 mm compares to a measured 6.15 mm. For ΔZ a maximum error of 0.18 mm (relative error of 18%) is found when ΔY-Ref = 1 mm, although for most values of ΔY, the absolute error in ΔZ is within 0.1 mm.

For ΔZ = 3 mm, as shown in Fig. 12, a maximum relative error of 2.8% is found, when an imposed displacement of −6mm is compared to a measured −5.83 mm. For ΔZ a maximum error of 0.27 mm (relative error of 9%) occurs when ΔY-Ref = -6mm, although for most ΔY the error in ΔZ is within 0.1 mm.

For ΔZ = 5 mm, as shown in Fig. 13, a maximum relative error of 2.2% is found, when an imposed displacement of 5 mm is compared to a measured 5.11 mm. For ΔZ a maximum error of 0.25 mm (5%) occurs when ΔY-Ref = -6mm, while for most ΔY the error in ΔZ is within 0.20 mm.

Secondly, the impact of imposed upward vertical displacement of ΔZ = -1, −3 and −5 mm are investigated. Negative ΔZ indicates that FP2 moves upwards and a relaxation of the optical fiber FL2 with respect to the (downwards) pretensioned state results. The results of each displacement step are shown in Figs. 14 to 16.

For ΔZ = -1mm, as shown in Fig. 14, a maximum relative error of 3% for ΔY is found, when an imposed displacement of −2mm is compared to a measured −2.06 mm. For ΔZ a maximum error of 0.17 mm (17%) occurs when ΔY-Ref = -1mm, while for most ΔY the absolute error in ΔZ remains within 0.15 mm.

For ΔZ = -3mm, as shown in Fig. 15, a maximum relative error of 6% is found for ΔY, at an imposed displacement of −1mm compared to a measured −1.06 mm. For ΔZ a maximum error of 0.18 mm (6%) occurs when ΔY-Ref = 2 mm, while for most ΔY the absolute error in ΔZ remains within 0.15 mm.

For ΔZ = -5mm, as shown in Fig. 16, a maximum relative error of 2.4% occurs for ΔY at an imposed displacement of 5 mm compared to a measured 5.12 mm. For ΔZ a maximum error of 0.47 mm (9.5%) occurs when ΔY-Ref = -5mm, while for most ΔY the absolute error of ΔZ is within 0.3 mm.

4.3. General accuracy assessment of designed DOFS system

As shown in the lab experiment results, the DOFS system can accurately detect two-directional joint displacements. But like any other type of sensor, measurement errors do occur. The results indicate a highly acceptable accuracy for measuring horizontal joint opening, as a maximum relative error of only 6% is found (for an imposed ΔZ = -3mm, ΔY = -1.06 mm when ΔY-Ref = -1mm). For most displacement steps, the relative error of ΔY remains below 2.5%. Under normal operational conditions where ΔY is expected to remain between −4mm and 4 mm, the absolute error is smaller than 0.1 mm, which means the DOFS can register relative joint openings as accurately as 0.1 mm. Also, for extreme deformation conditions where ΔY is within the range of (-6mm, −4mm) and (4 mm, 6 mm), the observed maximum absolute error is 0.15 mm (a relative error of only 2.5% when ΔZ = 1 mm, ΔY-Ref of 6 mm compared to a measured 6.15 mm).

For vertical differential settlements, the results show a more significant error. Especially for a scenario with limited uneven settlements,

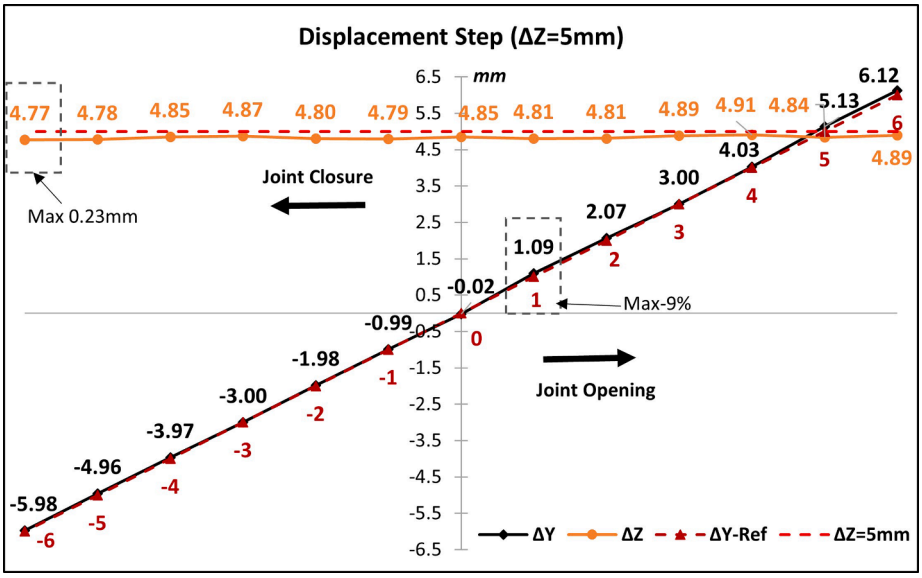

Fig. 9. Measurement result comparison of D-0.9 mm fiber (ΔZ = 5 mm).

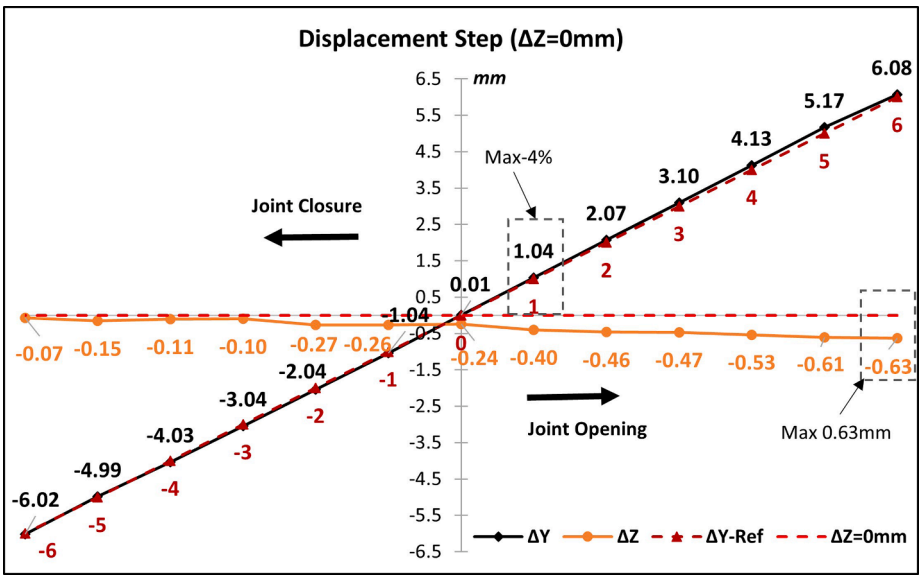

Fig. 10. Measurement result comparison (ΔZ = 0 mm).

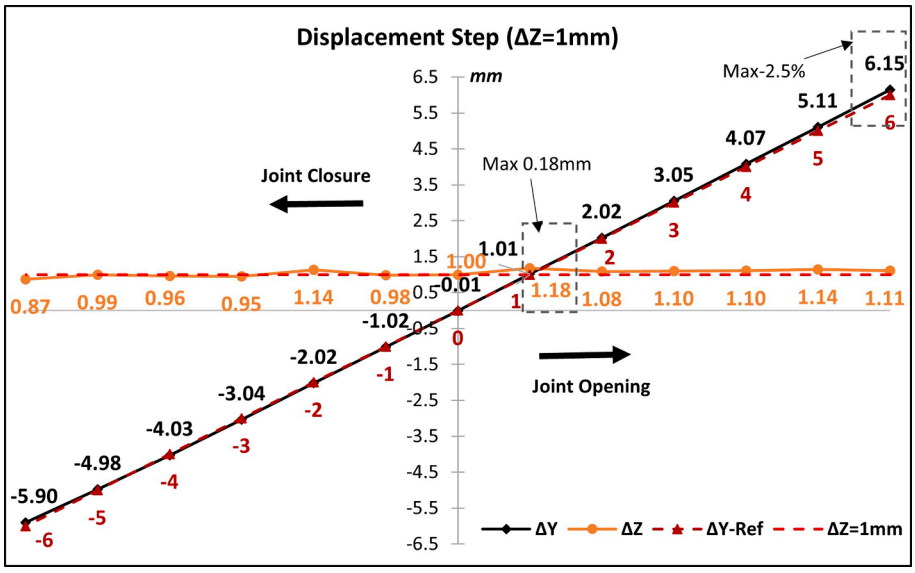

Fig. 11. Measurement result comparison (ΔZ = 1 mm).

where $\Delta Z = \pm 1mm$, the maximum relative error observed is 18% (when ΔZ = 1 mm while measured ΔZ = 1.18 mm). The maximum absolute error is found 0.47 mm (a relative error of 9.5%), which only occurs when ΔZ = -5mm while the measured ΔZ = -4.53 mm. However, for most imposed displacements, the measured displacement has a relative error below 10%, and absolute error below 0.3 mm, which is better than the reported accuracy of ±1 mm for manual levelling measurements. Despite a careful check and the experimental setup being assembled as accurately as possible, errors in the setup still exist. These error sources include: (1) a possible difference between the actual length of sensing fiber and the designed length, especially for the inclined fiber line FL2; (2) a small inclination of the fixed platform, which means the BP may not move in an absolutely horizontal plane in the test; (3) a small tilting of the vertical frame (where FP1 and FP3 are bonded) or vertical plate (VP in Fig. 9) under tension forces of FL2; (4) the stated accuracy of the BOFDA interrogator when collecting data. It should be noted that especially some limited tilting of VP and the vertical frame when imposing different displacement steps (which has been observed in the test) contribute most significantly to these errors, as the strain of FL2 is quite sensitive to even very small vertical movements caused by tilting. However, this error source is less likely to be present in the field tests, as the tensioned fiber will, of course, not be able to tilt the entire tunnel segment to which the fixture points are bonded.

In summary, the DOFS system is verified to have a more than acceptable accuracy and a good performance for subsequent field testing.

Of the two fiber types tested in the experiment, the D-2 mm optical fiber physically proves to have a moderate axial stiffness of about 3kN, which can be pre-tensioned easily while still adequately resistant to external impacts or damage due to handling during installation, compared with the thin D-0.9 mm fiber (Zhang and Broere, 2022). Therefore, the D-2 mm optical fiber is chosen for a subsequent field installation test in the First Heinenoordtunnel.

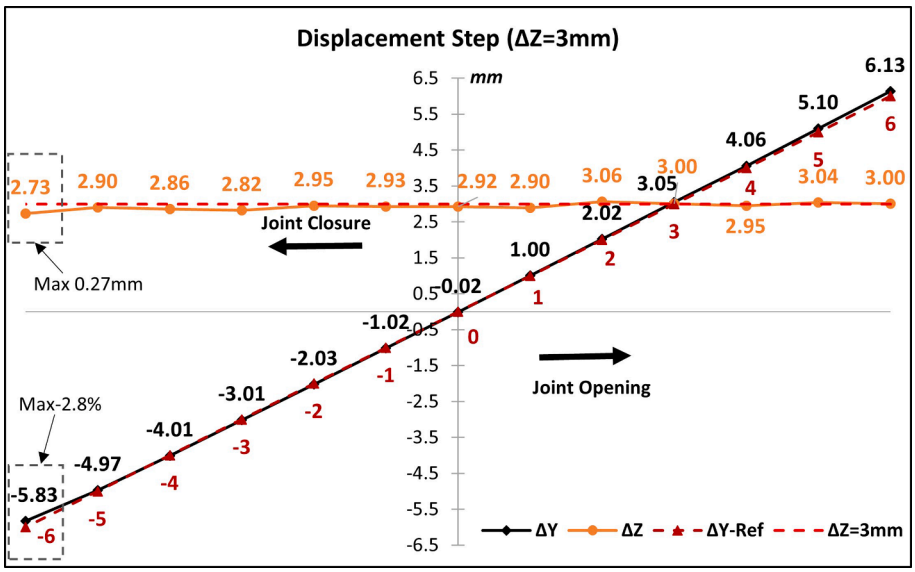

Fig. 12. Measurement result comparison (ΔZ = 3 mm).

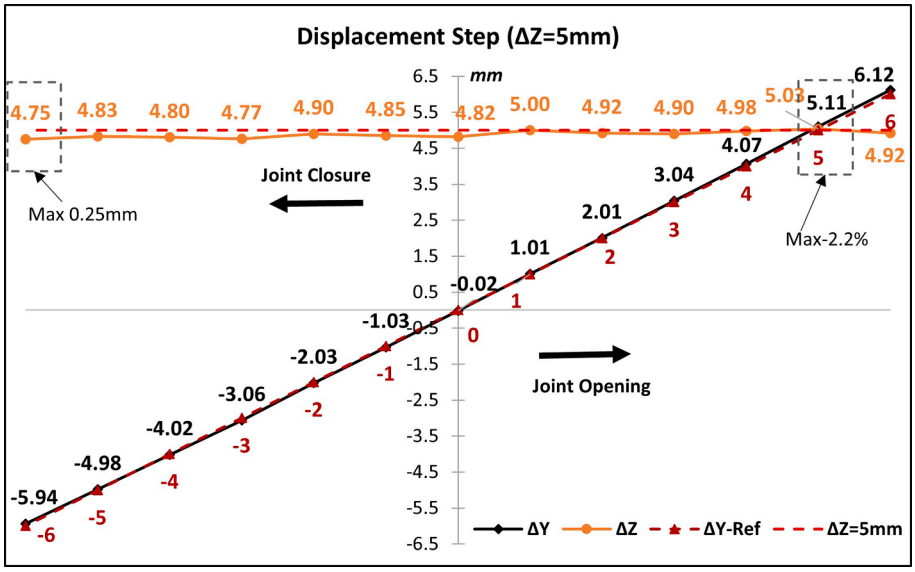

Fig. 13. Measurement result comparison (ΔZ = 5 mm).

5. Sensor installation at the first Heinenoordtunnel

5.1. Introduction of first Heinenoordtunnel

The distributed optical fiber sensor (DOFS) system is installed in the First Heinenoordtunnel in the Netherlands to show the applicability and robustness in field conditions. The First Heinenoordtunnel is a typical Dutch immersed tunnel and opened to service in 1969. It consists of 5 concrete elements each about 115 m long, which in turn consist of 6 segments each about 19 m long. The total length of the closed section is about 754 m, with the immersed section 574 m. The Heinenoordtunnel has 31 joints in total, including 25 dilation joints and 6 immersion joints, see Fig. 17.

Previous monitoring by manual levelling has shown that significant uneven settlement has occurred along the tunnel. Compared to the reference measurement in 1978, the maximum settlement equals about 67 mm at the middle of 1st element, and the minimum settlement is about 24 mm, which indicates a maximum settlement difference of about 43 mm longitudinally according to the measurement results for 2018. Only vertical settlement is monitored at a limited number of locations (next to each immersion joint and the center points of the elements) by conventional manual leveling with a minimum interval of 1 year. After a service period of more than 50 years, structural integrity of the tunnel structure has become an issue and for several joints the watertightness is a point of concern. Observations from similar immersed tunnels and from lab experiments show that seasonal temperature loading may negatively impact the structural safety, but no definitive measurements confirming or denying this behavior are available for the Heinenoordtunnel and a yearly or multi-year monitoring interval will not show such seasonal influences (Rahadian et al., 2018). Therefore, the DOFS system is designed to instrument all the joints of First Heinenoordtunnel and form a remote-controlled monitoring system which allows for high-frequency measurement while imposing no disturbance to tunnel service.

5.2. Field sensor installation and monitoring

Fig. 18 gives an impression of the sidewall of the west tube (North to

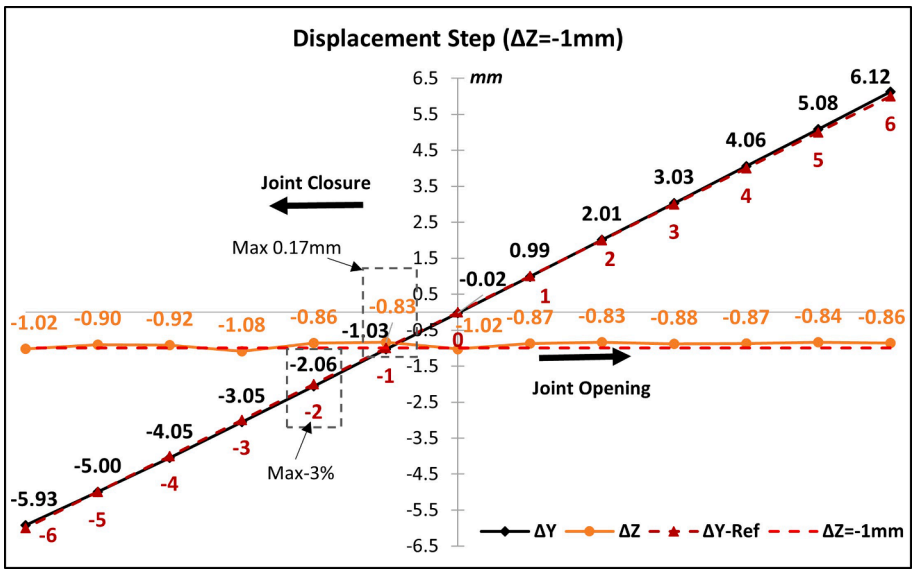

Fig. 14. Measurement result comparison (ΔZ = −1 mm).

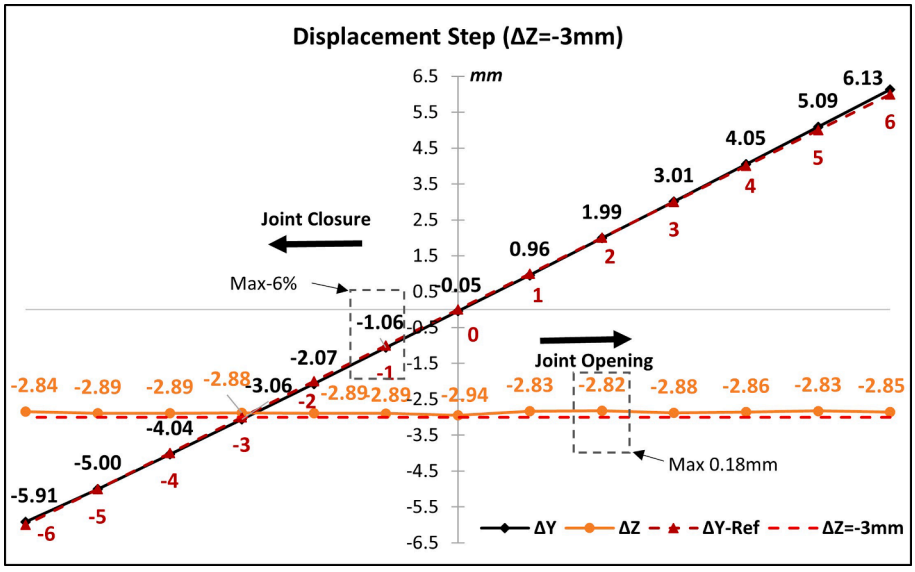

Fig. 15. Measurement result comparison (ΔZ = −3 mm).

South, from Rotterdam to Barendecht) which is to be instrumented with the DOFS system. The immersion joints and dilation joints have different dimensions and hence two different types of sensing layouts are designed.

To form a sensor block, the optical fiber shall be fixed at 3 points on the wall, such that two pre-strained fiber lines (FL1 and FL2 in Fig. 4) cross the joint gap. However, it is difficult or even impossible to directly bond the small optical fiber onto tunnel wall surface sufficiently accurate and leave a predetermined length of sensor fiber unbonded in between. The key problem is how to fix the fiber lines (FL1/FL2) as accurately as possible, while imposing a designated pre-strain at the same time, see Fig. 19(a). In addition, considering that the time for field installation is limited by the short tunnel maintenance windows, which occur at night only to limit traffic hindrance, work flow efficiency is highly important so as to reduce field installation duration.

To solve this dilemma, the optical fiber is pre-bonded to small pads at designated points, and thus assembled to form a sensor block, see Fig. 19 (b). The subsequent field installation will focus on fixing these pads at precise locations. In order to protect the bare sensor blocks and fibers on the wall, special cover boards have been made by cold-bending thin steel plate. These are installed over the sensors to fully isolate the sensor block from potential external impacts, see Fig. 19(c). It should be noted the fiber line 3 (FL3) in Fig. 19(a) is untensioned and aligned parallel to FL2 for sake of easy installation and protection. In each sensor block only FL1 and FL2 are pre-strained and function as joint displacement sensors.

The field installation in the First Heinenoordtunnel was limited to night tunnel closures with an effective working time of 3.5 h to install a continuous fiber loop with 31 sensor blocks. The unstressed optical fiber cable between each joint is buried into a long PVC duct which is fixed on top of the roadway barrier, see Fig. 20. The two fiber cable ends are extended outside the tunnel at the North portal and plugged into the BOFDA interrogator inside the service building. As the whole system can be remotely controlled, the installed DOFS system can obtain measurements at hourly or better intervals while imposing no disturbance to road traffic in the tunnel.

The installation procedure is robust enough to be handled even during the peak of the covid pandemic, although this has caused some delays and has put restrictions on the amount of personnel that could be

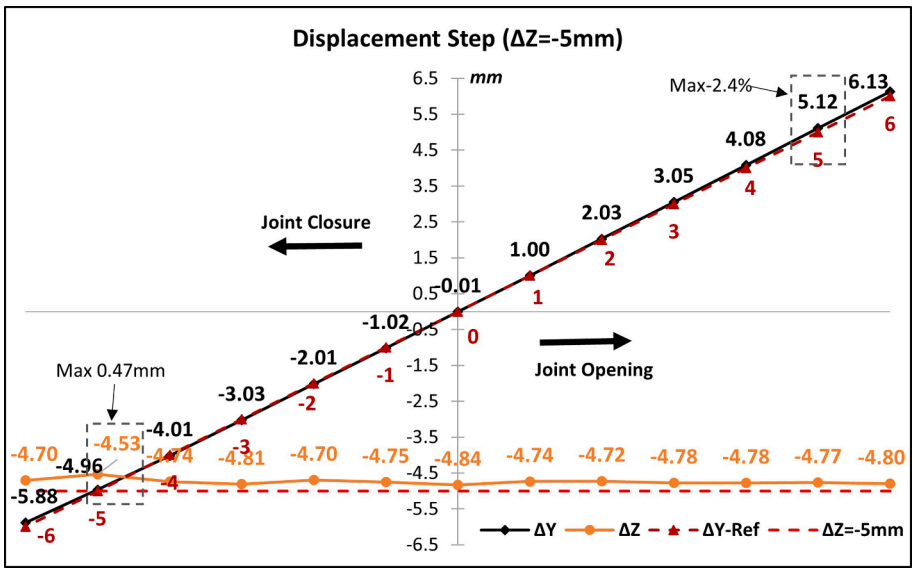

Fig. 16. Measurement result comparison (ΔZ = −5 mm).

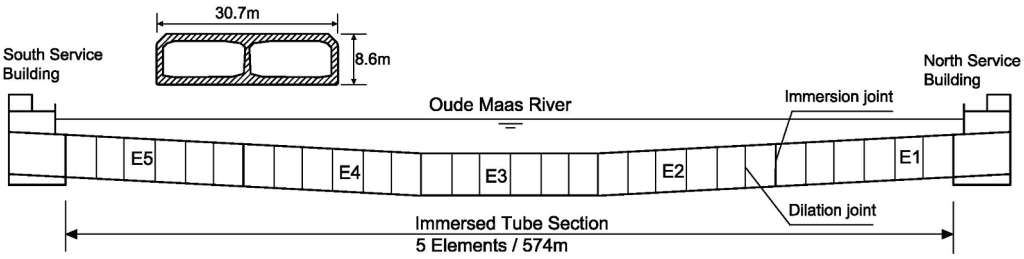

Fig. 17. Side view of the First Heinenoordtunnel.

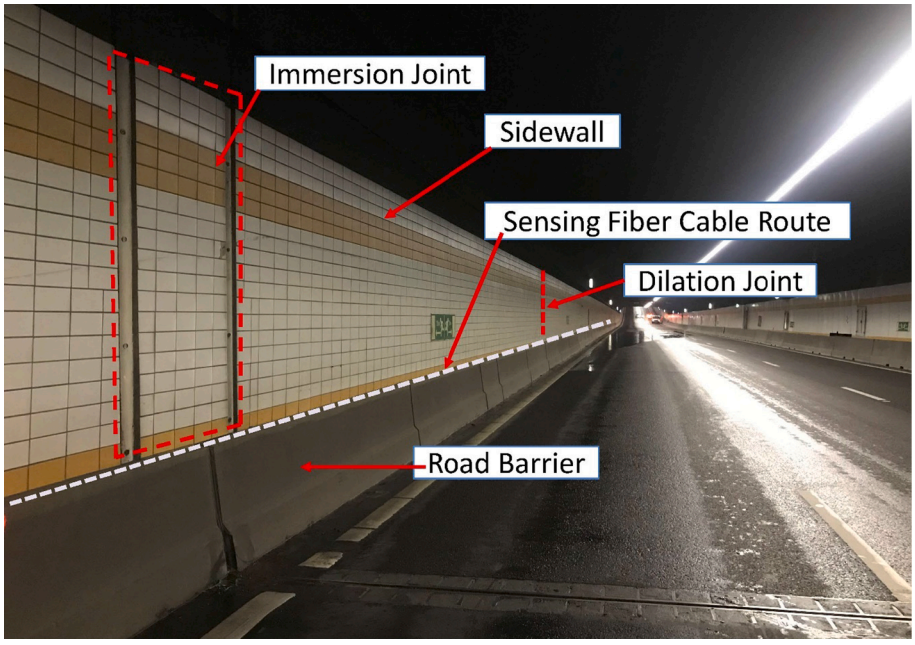

Fig. 18. Sidewall of west tube to be instrumented by DOFS.

used simultaneously to install the sensors. Therefore initially only half of the tunnel (3 immersion joints and 10 dilation joints) was instrumented.

As it can be expected that the temperature in the tunnel differs from the outside temperature, and differs along the tunnel length, the measured BFS of a short unstrained fiber section (of about 40 cm length) directly next to the strained fiber lines for each sensor block is used to

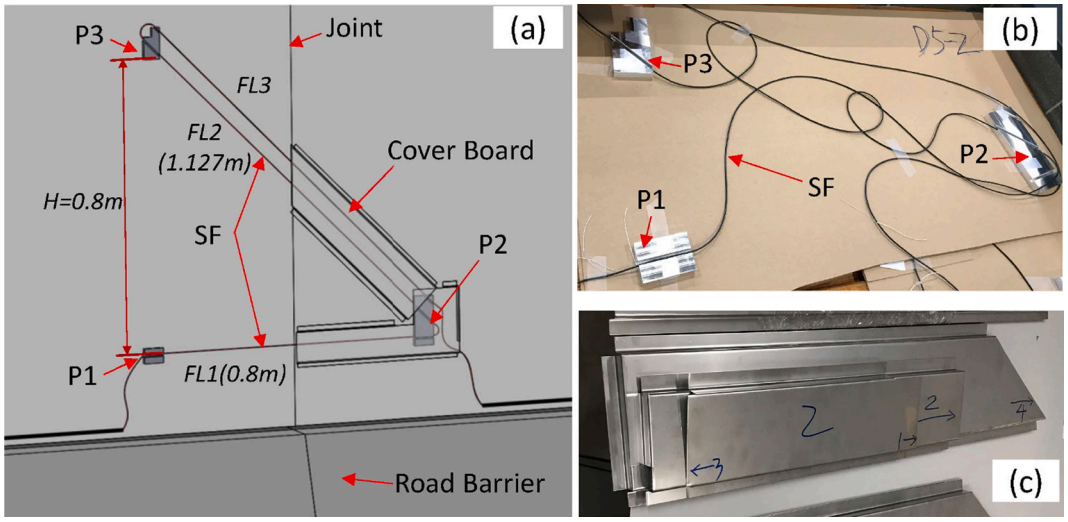

Fig. 19. Field sensor installation plan: (a) Sensor block installation plan at dilation joint; (b) indoor optical fiber-pad assembly; (c) cover boards for fiber sensor protection (Note: SF as sensing fiber).

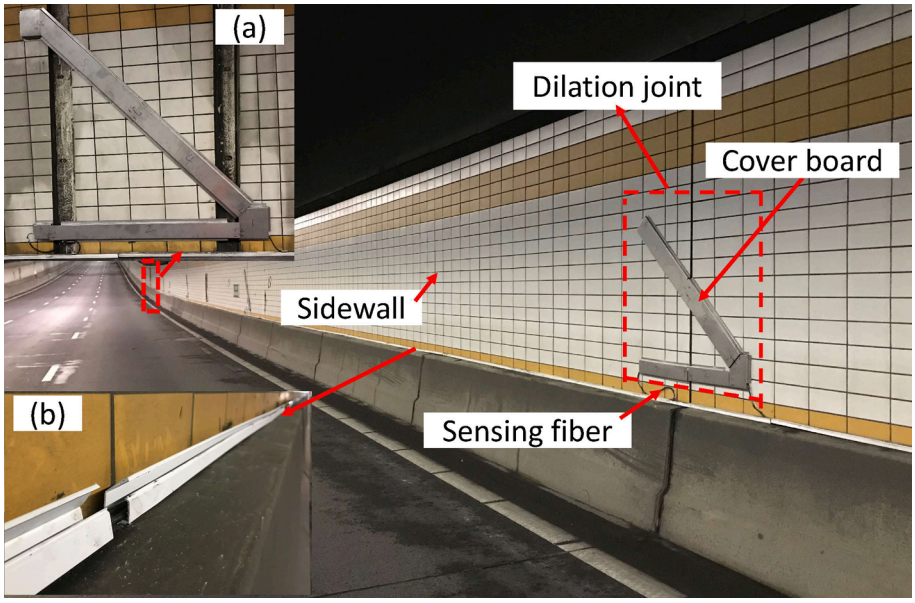

Fig. 20. Finished fiber sensor installation in the First Heinenoordtunnel:(a) Sensor at immersion joint;(b) Loose fiber in PVC duct;

calculate the temperature using Eq. (16):

$$T = T_0 + (\Delta f_{t,i})/C_t \tag{16}$$

where C_t is the temperature sensitivity coefficient, determined as 1.89 MHz/°C; $\Delta f_{t,i}$ is the measured BFS change (at interval) relative to that at reference temperature T_0 (here 22.8 °C).

To verify the accuracy, the measured temperature at the first immersion joint (near the north portal of the Heinenoordtunnel) is compared with the outside temperature (daily mean, from Meteoblue, 2022) observed in the Heinenoord area. As shown in Fig. 21, the DOFS temperature measurements during the first week of January 2021 agree very well with the outside temperature, and the difference between is within 1 degree, which indicate the measurement accuracy of the installed DOFS system is acceptable.

Fig. 22 shows the measured temperature and joint deformation result (daily mean) derived from the measured BFS using Eqs. (2) to (15) for the first immersion joint (North) during the first 47 days after the system had been installed. The baseline is set to 11 Dec. 2020, and it can be seen

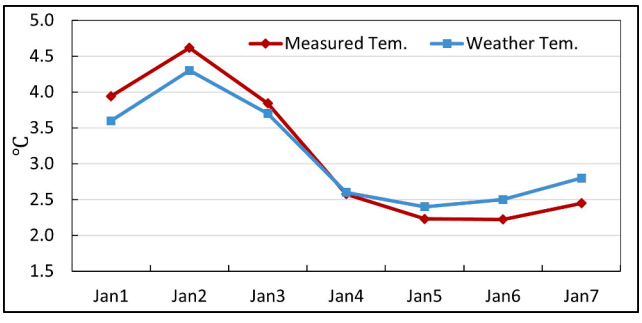

Fig. 21. Comparison between measured temperature at the first immersion joint and outside weather temperature.

that within the observation period the joint deformations (absolute) are within 1 mm, and they show a variation with temperature. The joint opening shows a high negative correlation with temperature (the

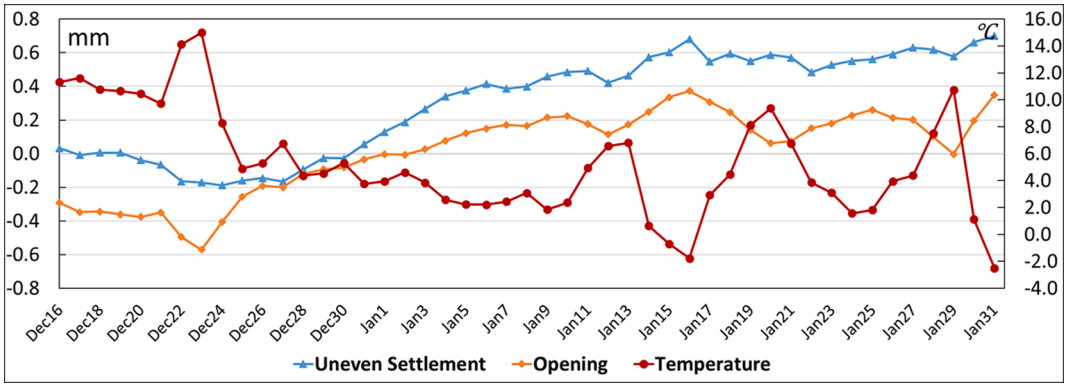

Fig. 22. Measured joint deformation of the first immersion joint.

Pearson correlation coefficient is −0.84), indicating the joint tends to open at decreasing temperature while to close at increasing temperature. This is consistent with the observation that thermal expansion of the segments can be compensated by cyclic joint opening (Bai and Lu, 2016); The joint uneven settlement also shows variation with temperature (the Pearson correlation coefficient is −0.57, lower than that of the joint opening), which indicates the small vertical deformation at this joint is partially influenced by the temperature effects.

In summary, the designed DOFS monitoring system is able to detect two-directional joint deformation (joint opening and uneven settlement) in field conditions. A longer period monitoring study to obtain the tunnel behavior for a full seasonal cycle is now underway.

6. Conclusions

DOFS is able to measure continuously distributed strain and temperature along an optical fiber and has a high potential in structural monitoring systems. A distributed optical fiber sensor has been designed to acts as a joint displacement monitoring system for an immersed tunnel.

The exact optical fiber sensor layout is designed based on the relation between measured fiber strains and the actual joint displacements. For the specific layout used, the accuracy has been verified by a lab experiment first. Results show this can effectively monitor two-directional joint deformations with more than acceptable accuracy. Sub-millimeter deformations of the tunnel can be well captured by the DOFS, and for monitoring of horizontal joint opening or closure, a maximum relative error of 6% (absolute error of 0.09 mm) is found while in most cases the error remains below 2.5%. For vertical uneven settlement, in cases with small relative settlements of ± 1 mm, the maximum absolute error observed in the lab experiments is 0.18 mm, while for most cases the measured displacement has a relative error below 10% and an absolute error below 0.5 mm. This study shows the DOFS system has an acceptable accuracy for joint displacement monitoring in field conditions.

Subsequently, the DOFS has been successfully installed to instrument both immersion joints and dilation joints at the First Heinenoordtunnel in the Netherlands, and data collection has started. Monitoring results for a full seasonal cycle showing the impact of temperature change on the tunnel construction will be available in the near future, but initial results show the system is capable of delivering daily (and even hourly) deformation readings for the instrumented joints. This shows a major improvement in the capabilities to monitor actual tunnel deformations in real-time.

CRediT authorship contribution statement

Xuehui Zhang: Methodology, Investigation, Visualization. **Wout Broere:** Conceptualization, Supervision, Funding acquisition.

Declaration of Competing Interest

The authors declare that they have no known competing financial interests or personal relationships that could have appeared to influence the work reported in this paper.

Acknowledgements

This research has been financially supported by China Scholar Council (China) and Rijkswaterstaat, the Netherlands. The authors thank Rijkswaterstaat for granting the access to the tunnel and the installation of the sensors.

References

Acikgoz, S., Pelecanos, L., Giardina, G., Aitken, J., Soga, K., 2017. Distributed sensing of a masonry vault during nearby piling. Struct. Control Health Monit. 24, e1872.
Bai, Y., Lu, H., 2016. Damage Analysis and Repair Technology of OMEGA Gasket in Immersed Tube Tunnel. J. Railw. Eng. Soc. 9, 87–92. In Chinese.
Berkhout, B.J., et al. 2014. Instandhouding zinkvoegen. Technical report T330, COB, Delft, The Netherlands. https://www.cob.nl/document/instandhouding-zinkvoegen/.
Fibristerre (2021), Information of BOFDA interrogator see https://www.fibristerre.de/files/fibrisTerre_flyer.pdf (latest accessed in June 2021).
Gavin, K.G., Broere, W., Kovačević, M.S., de Haas, K., 2019. Investigation of the remaining life of an immersed tube tunnel in The Netherlands. In: ProceedIngs of the WTC 2019 ITA-AITES World Tunnel Congress, p. 4831.
Grantz, W.C., 2001. Immersed tunnel settlements: Part 2: case histories. Tunn. Undergr. Space Technol. 16 (3), 203–210.
Gue, C.Y., Wilcock, M., Alhaddad, M.M., Elshafie, M.Z.E.B., Soga, K., Mair, R.J., 2015. The monitoring of an existing cast iron tunnel with distributed fibre optic sensing (DFOS). J. Civil Struct. Health Monit. 5, 573–586.
Li, W., Wu, D., Guo, X., Gao, X., 2011. Overhaul Design and Construction of Ningbo Yongjiang Immersed Tube Tunnel. Modern Tunn. Technol. 48 (1), 81–89. In Chinese.
López-Higuera, J.M., Cobo, L.R., Incera, A.Q., Cobo, A., 2011. Fiber optic sensors in structural health monitoring. J. Lightwave Technol. 29 (4), 587–608.
Lunniss, R., Baber, J., 2013. Immersed tunnels. CRC Press.
Meteoblue, 2022. Meteoblue weather report information. https://www.meteoblue.com. (Accessed May 2022).
Mohanad, H., Bennett, P.J., Soga, K., Mair, R.J., Bowers, K., 2010. Behaviour of an old masonry tunnel due to tunneling-induced ground settlement. Geotechnique 60 (12), 927–938. https://doi.org/10.1680/geot.8.P.074.
Motil, A., Bergman, A., Tur, M., 2016. State of the Art of Brillouin Fiber-Optic Distributed Sensing. Opt. Laser Technol. 78, 81–103.
Ohno, H., Naruse, H., Kihara, M., Shimada, A., 2001. Industrial Applications of the BOTDR Optical Fiber Strain Sensor. Opt. Fiber Technol. 7 (1), 45–64.
Pelecanos, L., Soga, K., Elshafie, M.Z.E.B., de Battista, N., Kechavarzi, C., Ye Gue, C., Ouyang, Y., Seo, H., 2018. Distributed fiber optic sensing of axially loaded bored piles. J. Geotech. Geoenviron. Eng. 144, no. 3.
Rahadian, R., van der Woude, S., Wilschut, D., Blom, C.B., Broere, W., 2018. A new test setup for studying sand behaviour inside an immersed tunnel joint gap. InPhysical Modelling in Geotechnics. CRC Press, pp. 443–448.
Saveur, J., Grantz, W., 1997. Structural design of immersed tunnels. Tunn. Undergr. Space Technol. 12 (2), 93–109.
Schwamb, T., Soga K., Mair, R.J., Mohammed Z. E. B. Elshafie, Sutherden R., Bouquet C., and Greenwood J., 2014. Fibre Optic Monitoring of a Deep Circular Excavation. Proceed. Inst. Civil Eng. – Geotech. Eng. 167, no. 2, 144–154.
Van Montfort, R., 2018. Insufficiency of immersion joints in existing immersed tunnels: Case study on functioning of Gina-seal and Omega-seal in the Kil Tunnel. Delft University of Technology, Delft, The Netherlands. MSc Thesis.

Wang, X., Shi, B., Wei, G., Chen, S., Zhu, H., Wang, T., 2018. Monitoring the behavior of segment joints in a shield tunnel using distributed fiber optic sensors. Struct. Control Health Monit. 25, e2056.
Wang, S., Zhang, X., Bai, Y., 2020. Comparative study on foundation treatment methods of immersed tunnels in China. Front. Struct. Civil Eng 14 (1), 82–93.
Zhang, X., Broere, W., 2022. Sensing Fiber Selection for Point Displacement Measuring with Distributed Optic Fiber Sensor. Measurement 197, 111275. https://doi.org/10.1016/j.measurement.2022.111275.
Zhu, H.H., Wang, D.Y., Shi, B., Wang, X., Wei, G.Q., 2022. Performance monitoring of a curved shield tunnel during adjacent excavations using a fiber optic nervous sensing system. Tunnelling and Underground Space Technology 124, 104483.